IEEE Access
Multidisciplinary | Rapid Review | Open Access Journal

Received September 30, 2020, accepted October 18, 2020, date of publication October 23, 2020, date of current version November 5, 2020.

Digital Object Identifier 10.1109/ACCESS.2020.3033485

A High-Speed Microturbine PMa-SynRG Emulation Using Power Hardware-in-the-Loop for Wind Energy Conversion Systems

FAYEZ F. M. EL-SOUSY[1], (Member, IEEE), GHADA A. ABDEL AZIZ[2], (Member, IEEE), MAHMOUD AMIN[2,3], (Senior Member, IEEE), KHALED GABER[4], AND OSAMA A. MOHAMMED[5], (Life Fellow, IEEE)

[1]Department of Electrical Engineering, College of Engineering, Prince Sattam bin Abdulaziz University, Al-Kharj 16278, Saudi Arabia
[2]Power Electronics and Energy Conversion Department, Electronics Research Institute, Cairo 333031, Egypt
[3]Electrical and Computer Engineering Department, Manhattan College, Manhattan, NY 10471, USA
[4]Department of Electrical Engineering, Faculty of Engineering, Al-Azhar University, Cairo 11651, Egypt
[5]Electrical and Computer Engineering Department, Florida International University, Miami, FL 33174, USA

Corresponding author: Ghada A. Abdel Aziz (ghada_ahmed@ieee.org)

The authors extend their appreciation to the Deputyship for Research and Innovation, Ministry of Education in Saudi Arabia for funding this research work through the project number ID:1289.

ABSTRACT In this paper, a high-speed microturbine (MT) permanent magnet assisted synchronous reluctance generator (PMa-SynRG) real-time emulation based on linear impedance regulator (LIR) using power hardware-in-the-loop (PHIL) for wind energy generation tests is presented. The LIR is designed without any feedback control loop for reshaping the *s*-domain performances of the current filter along with the converter inside the PMa-SynRG emulated system. The PHIL platform not only provides a method for eliminating the high cost of using real renewable energy hardware but also it enables the developers to create new, rapid, and reliable controllers for renewable energy testing. This platform can be used in investigating the performance of energy system under various conditions even if the generator prototype is not yet developed or unavailable. PMa-SynRG mathematical model is emulated in the real-time using PHIL platform while the output voltage of the proposed emulator imitates the generated voltage through the simulated model. In addition, a voltage source converter is employed as a voltage amplifier for imitating the PMa-SynRG performance when supplying nonlinear/linear loads. In this paper, the proportional-integral resonant (PIR) controller is utilized at the voltage control loop for tracking the distorted output reference signal voltage. In order to investigate the performance of the proposed PMa-SynRG emulator, it has been simulated and compared with MATLAB/SIMULINK environment.

INDEX TERMS Permanent magnet assisted synchronous reluctance generator, power hardware-in-the-loop, real-time emulation, microturbine.

NOMENCLATURE

V_a, V_b, V_c	PMa-SynRG stator three-phase voltages
I_a, I_b, I_c	PMa-SynRG stator three-phase currents
I_s	PMa-SynRG stator current
V_{ds}, V_{qs}, I_{ds}, I_{qs}	PMa-SynRG stator *dq* voltages and currents
L_E	Stator leakage inductance
L_d, L_q	*dq* inductances per phase
λ_d, λ_q	*dq*-axis flux-linkages
λ_{PM}	PM flux linkage
R_s, L_s	Stator resistance and inductance
P	Number of pair poles
ω_r	Rotor mechanical angular speed
ω_r^*	Rotor reference speed
θ_r	Rotor position angle
T_e	Electromagnetic torque
T_{mech}	Mechanical torque
T_b, P_b, ω_b	MT base torque, power, and speed
J	Moment of inertia
R_L	Equivalent Thévenin 3-phase resistances
V_{DC}	DC-link voltage
L_f, C_f, R_f	Filter inductor, capacitor, parasitic resistor
t	Time

The associate editor coordinating the review of this manuscript and approving it for publication was Atif Iqbal.

I. INTRODUCTION

Due to their simple structure, high power density, small size, and high torque-to-inertia ratio, permanent magnet assisted synchronous reluctance machines (PMa-SynRMs) have been extensively used in various industrial applications e.g. aerospace, robotics, and CNC machine tools [1]–[3]. Permanent magnet assisted synchronous reluctance generator (PMa-SynRG) in near future will be considered one of the most promising generators in the wind energy conversion system (WECS) due to its self-excitation, high efficiency and high reliability features [4]. Moreover, it needs lower maintenance due to its gearless construction [5]. PMa-SynRGs can provide whole isolation from the disturbances of the grid owing to their fully rated converters as they are less susceptible to the faults of the grid as well can efficiently support the grid during different fault conditions [6].

For larger traction applications, e.g. electric aircrafts or ship-propulsion systems, the permanent magnet generator is employed as a part of the mobile power system for supplying the power to numerous subsystems in the vehicle [7].

For generator as well as motor drive applications, the machine is optimally designed to enhance safety, efficiency, compactness, and maintainability in an identical frame, thus, the designation process is confirmed through standard test in which real hardware testing is often desired for guaranteeing functionality along with reliability. For instance, an electric machine with flywheel has been presented in [8] for investigating the motor drives reliability, as well as [9] employed the electric motors for the examining the IGBT modules in the electric vehicles. These machine-based approaches have faced various limitations to encounter the emerging requirements: e.g. the high-power electric machines which are bulky, mechanical loads which are hard to recreate, along with the machine-based investigation setups could be very luxurious to build. In the emulation system, the power electronics converters are employed for generating similar electrical performances to electric machines, as well as the mechanical performances are calculated via employing digital controllers. Indeed, during performing new tests on electric machines as well as power electronic devices, serious damage or faults may occur on this equipment. Therefore, for operating in safe-mode, real-time emulation platform such as power hardware-in-the-loop (PHIL) is employed to perform various tests [10], [11].

PHIL emulator is a powerful platform that is employed for validating and testing the machine-drive system components such as control approaches and power electronic converters [12]. This platform can solve various problems occur in real hardware implementation e.g. nonlinearity of inverter or power amplifiers, the interface of sensor noise produced by switching of semiconductor switches, real-time numerical convergence problems caused by circuit solvers which may lead to latency and instability of the system [13].

The PHIL can solve the previous stated problems; as well it is considered as a feasible solution for investigating drive system performance in transportation and electric vehicle applications [14], [15]. Furthermore, via employing the PHIL, the hardware component can interact with simulated devices as well as the mathematical modeling of the system which is not physically present. Moreover, the PHIL has the feature of testing the system with real parameters and loads in real-time [16].

Various published papers have been concentrated on the virtual machines implementation in [17], [18]. Indeed, [19], [20] have been concentrated on the emulation of induction motor (IM), [21]–[23] presented the emulation of conventional PM machines in the motoring mode. Nevertheless, few papers dealt with the emulation of the PM machine in the generator mode [24], [25] and the emulation of PMa-SynRG has not discussed before. Therefore, this paper presents the detailed emulation design of a high-speed MT PMa-SynRG using the PHIL for wind energy generation tests. The detailed block diagram of the PMa-SynRG-based WECS is depicted in Fig. 1. This block comprises the PMa-SynRG coupled with the microturbine (MT), the PMa-SynRG side converter, the grid side converter, the LC filter, along with the three-phase load.

This paper is structured as follows: Section II presents the integration of the PMa-SynRG with the MT. The configuration of the emulator system is addressed in Section III. The experimental investigation is introduced in Section IV. Section V finally concludes this paper.

II. PMa-SynRG AND MT INTEGRATION SYSTEM

In the high-speed single-shaft MT integrated with the PMa-SynRG design, both the MT along with the compressor are mounted on the same shaft for high efficiency operation.

A. PMa-SynRG FEA TOPOLOGY

The PMa-SynRG topology with parameters in Table 1 has concentrated 3-phase windings, laminated rotor core along with segmented magnets as illustrated in Fig. 2. As depicted, both the stator and rotor iron cores are supposed to be infinitely permeable. Fig. 3 illustrates the FEA model of the PMa-SynRG with the flux density plot. As illustrated, the PMa-SynRG has a 3/8 pitch windings with 16 magnets along with 18 stator slots. As shown in Fig. 2, the stator teeth are straight. For intensive employment of the reluctance torque, flux barriers contains three-layers as well amassed in the rotor radial direction for affording the large design liberty for saliency ratio. Fig. 4 shows the flux-density distribution at maximum PMa-SynRG current with negative d-axis current. This figure presents the numerical simulation result of a half repetitive machine section. The negative field-weakening current can cause a high irreversible demagnetization particularly of the 2nd magnet from the left. Consequently, the operation at a high negative d-axis current must be banned for evading the degradation of the PMa-SynRM operation.

As the d-q inductances of the PMa-SynRG are not constant, they are obtained via the FEA. Fig. 5a along with Fig. 5b

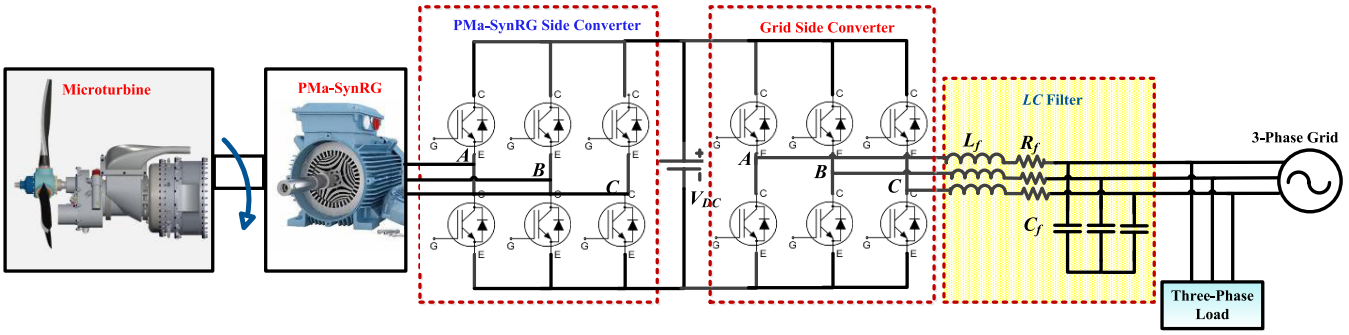

FIGURE 1. The block diagram of the PMa-SynRG-based WECS.

TABLE 1. Parameters of PMa-SynRG.

Rated power	50 kW	Stator resistance	0.56 Ω
Line voltage	1.7 kV	q-axis inductance	18.5 mH
Rated current	17.3 A	d-axis inductance	3 mH
Rated torque	12.2N.m	Friction coefficient	0.00018 N.m.sec/rad
Base frequency	1114 Hz	Bottom radius of slots	18.75 mm
Pair poles	4	Inner stator diameter	116 mm
Inner radius of rotor	7.5 mm	Stack length	65 mm
Outer radius of rotor	14.5 mm	Active length of motor	48 mm
Inner stator radius	17.3 mm	Slot opening	1.2 mm

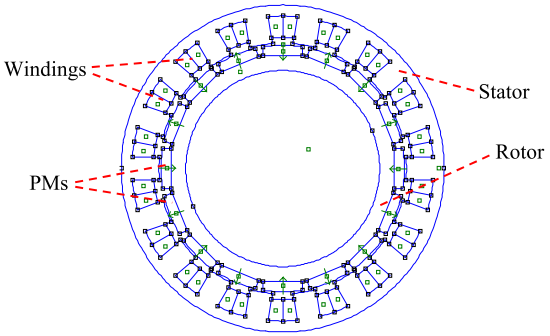

FIGURE 2. The PMa-SynRG model topology.

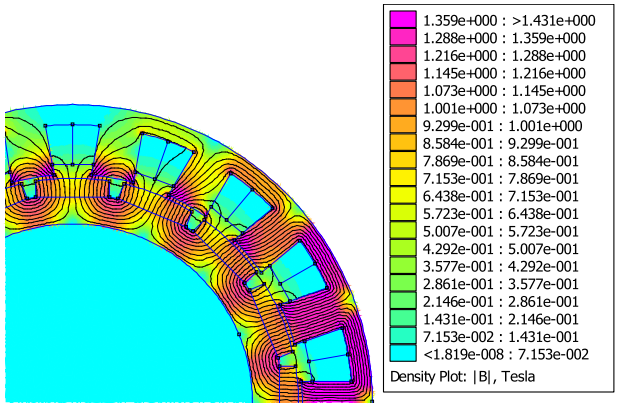

FIGURE 3. The PMa-SynRG FEA model with 3/8 pitch windings.

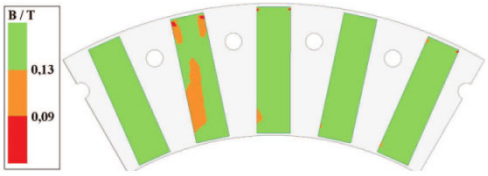

FIGURE 4. The flux density FEA result of the permanent magnet at the maximum negative d-axis current.

illustrate the FEA simulation results of the L_d versus I_d as well L_q versus I_q, respectively. As shown, the increment in the magnetic flux saturation can minimize the L_q as well L_d. The PMa-SynRG saliency ratio can be defined as L_d over L_q. At the PMa-SynRG rated current of 17.3 A (RMS), the I_q rated current is 11.35 A as well the I_d rated current is 13.06 A. At 200% of the rated I_d current of (34.6 A), the saliency ratio decreases nearby 30% (saliency ratio 3.6 to 2.6), which decreases the PMa-SynRG reluctance torque. The cross-saturation effect is remarkably prominent and supplementary decreases the reluctance torque.

B. PMa-SynRG MATHEMATICAL MODEL

Fig. 6 depicts the finite element analysis (FEM) structure of PMa-SynRG with a power factor corrected load connected to a converter for giving a purely resistive load response on the PMa-SynRG stator terminals [26]. For deriving the mathematical representation of the PMa-SynRG in the dq-reference frame, the following assumptions are considered:

1) Neglecting the hystresis losses and the eddy currents.
2) Considereing the back EMF to be sinusoidal.
3) Ignoring the saturation effect while it is considered via the PMa-SynRG parameters change.

The previous assumptions are adequate precise for describing the PMa-SynRG performance at healthy operation of the generator.

The mathematical equations of the PMa-SynRG can be expressed by (1) and (2):

$$\frac{dI_{ds}}{dt} = \frac{V_{ds}}{L_d} - \frac{R_s}{L_d} I_{ds} + P\frac{\omega_r}{L_d}\lambda_q \tag{1}$$

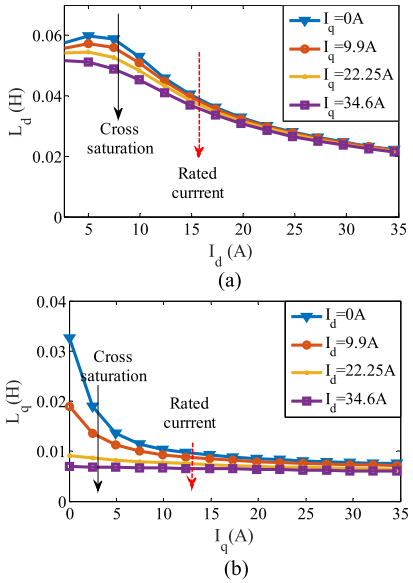

FIGURE 5. L_d and L_q calculations of the PMa-SynRG. (a) L_d vs. I_d (c) L_q vs. I_q.

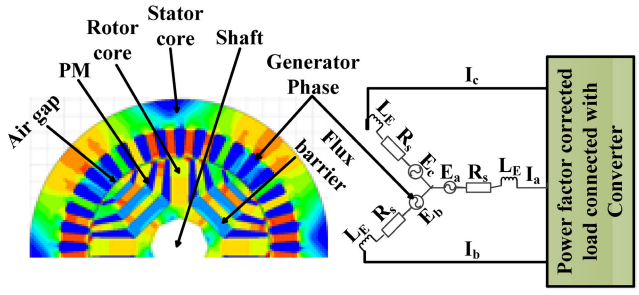

FIGURE 6. PMa-SynRG structure with a power factor corrector connected to converter using FEM.

$$\frac{dI_{qs}}{dt} = \frac{V_{qs}}{L_q} - \frac{R_s}{L_q} I_{qs} - P\frac{\omega_r}{L_q}\lambda_d \tag{2}$$

where $\lambda_q = L_q I_{qs} - \lambda_{PM}$ and $\lambda_d = L_d I_{ds}$.

The electromagnetic torque T_e can be represented by (3):

$$T_e = \frac{3P}{2} \times [\lambda_{PM} I_{ds} - (L_d - L_q) I_{ds} I_{qs}] \tag{3}$$

The PMa-SynRG rotor position angle can be calculated by (4):

$$\theta_r = \int \omega_r \cdot dt \tag{4}$$

It is recognized that the magnetic saturation can affect the PMa-SynRG performance especially in the q-axis, thus, L_d is not affected by saturation affects [2], [27]. Though, in the d-axis, the magnetic saturation has a distinct effect on the PMa-SynRG phase currents magnitude at low speeds operation, thus, this paper deals with high-speed PMa-SynRG.

C. MT MODEL

The mathematical model of the MT system presented in this paper is based on the model of gas turbine introduced by

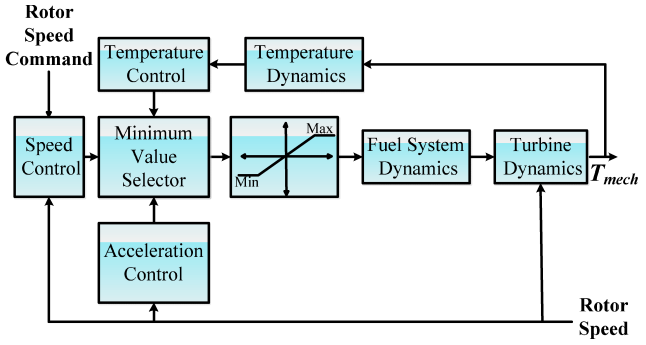

FIGURE 7. The MT model block diagram.

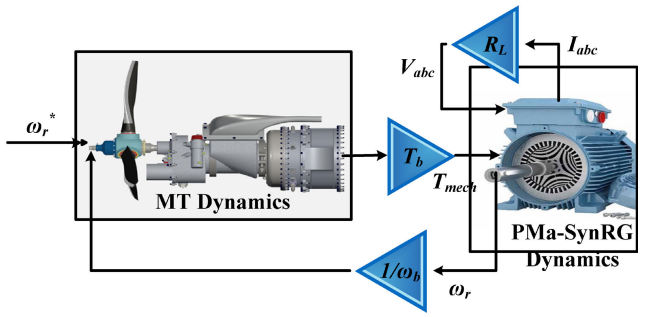

FIGURE 8. Integration of MT with PMa-SynRG.

Rowen in [28]. Fig. 7 depicts the MT model block diagram. As illustrated, the PMa-SynRG rotor speed command is the input to the system as it is determined according to the dynamics of both the MT and the generator. The MT model has three control loops as well as a minimum value selector. This selector is used for sending forward the smallest value of each of the three control loops meanwhile, the speed control loop is considered the active control. According to the temperature control, it takes over in case high temperatures are obtained and is repeatedly active in prolonged times of high-power rating activity. Afterwards, the subsequent value is passed over Min/Max limit which corresponds to the fuel consumption competence of the MT [23].

Subsequently, a series of transfer functions (TFs) consistent to fuel system, the valve positioner, and compressor delay is employed for determining the energy into the MT dynamics and calculating the torque applied on the shaft as this torque will be applied to the PMa-SynRG model.

D. INTEGRATING THE MT TO THE PMa-SynRG

Fig. 8 depicts the integration of the MT to the PMa-SynRG model. The PMa-SynRG rotor angular speed can be calculated by (5):

$$\omega_r = \frac{1}{J} \int (T_e + T_{mech}) \ .dt \tag{5}$$

In addition, the output torque on the shaft should be converted into actual torque via multiplying by T_b as expressed

by (6):

$$T_e = \frac{P_b}{\omega_b} \tag{6}$$

Afterwards, the converted actual torque is passed into the PMa-SynRG dynamic calculations. It is noted that, the input stator voltage to the PMa-SynRG dynamics depends on the R_L through the PMa-SynRG stator.

III. CONFIGURATION OF EMULATOR SYSTEM

The PHIL emulator architecture comprises a voltage source converter voltage amplifier which is used for converting the control signals of the numerical data within the processor into physical power handling nodes and the emulated PMa-SynRG model based on the LIR. In this paper, the voltage amplifier represents a two-level voltage source converter coupled with a 3-phase *LC* filter. This filter is employed for filtering switching voltage produced by the pulse width modulation at the terminals of the voltage source converter.

A. PMa-SynRG EMULATED MODEL BASED ON LIR

For the current-response mode, the terminal voltage is sampled into the controls of the PMa-SynRG emulator. The response of the reference current is acquired via the PMa-SynRG mathematical model, as well the current controller is employed for regulating the output current performances of the emulating converter. As the current control loop for the PMa-SynRG emulator has negative effects to the PMa-SynRG emulation performance, thus, this paper solves this problem via getting rid of this extra control loop within the PMa-SynRG emulator on the PHIL. The linear impedance regulator (LIR) is employed for generating the current response of emulating converter.

The transfer function (TF) from the terminal voltage to the current of the interface filter along with the PMa-SynRG stator can be designated as $G_f(s)$ as well as $G_s(s)$, which are represented via *RL* systems. For reshaping $G_f(s)$ into $G_s(s)$, the TF of the employed regulator $G_r(s)$ can be expressed by (7):

$$G_r(s) = \frac{G_s(s)}{G_f(s)} = \frac{sL_f + R_f}{sL_s + R_s} \tag{7}$$

In the PMa-SynRG emulator, it is obvious that the TF $G_r(s)$ also signifies the conversion from the voltage drop V_{Ls} on the PMa-SynRG stator impedance to the voltage drop V_{Lf} on the interface filter of emulating converter as expressed in (8):

$$G_r(s) = \frac{\left(sL_f + R_f\right) \cdot I_s}{(sL_s + R_s) \cdot I_s} = \frac{V_{L_f}}{V_{L_s}} \tag{8}$$

Fig. 9 depicts the PMa-SynRG emulator block diagram based on the LIR. According to the frequency-domain TF from the input voltage V_s to the PMa-SynRG stator current I_s, the cascaded system of the LIR as well as the interface filter should be equivalent to the PMa-SynRG stator, if the control delay and the sampling filter are ignored.

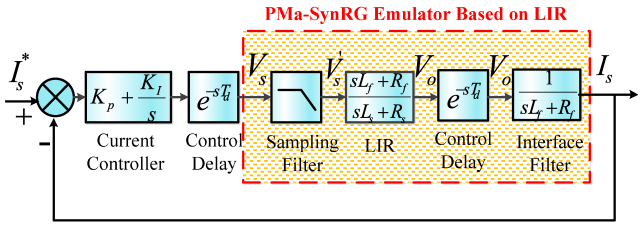

FIGURE 9. Block diagram of PMa-SynRG emulator based on LIR.

The PMa-SynRG emulator terminal voltage is sampled for impedance regulation, as well as the modulation wave V_o are generated via the LIR for regulating the emulating converter output current. Once the regulator is cascaded with the interface filter, the entire emulator will act correspondingly to the PMa-SynRG for the connected drive converter.

Both (1) & (2) of the PMa-SynRG can be rewritten in the *s*-domain in the form of (9) & (10), respectively:

$$V_{ds}(s) = (R_s + sL_d)\, I_{ds}(s) - P\omega_r(s)L_q I_{qs}(s) + P\lambda_{PM}\omega_r(s) \tag{9}$$

$$V_{qs}(s) = \left(R_s + sL_q\right) I_{qs}(s) + PL_d\omega_r(s)I_{ds}(s) \tag{10}$$

The PMa-SynRG stator voltage drop in the *dq*-frame V_{Lds} & V_{Lqs} can be expressed by (11)& (12), respectively:

$$\begin{aligned} V_{Lds}(s) &= (R_s + sL_d)\, I_{ds}(s) \\ &= V_{ds}(s) + P\omega_r(s)\, L_q\, I_{qs}(s) - P\lambda_{PM}\, \omega_r(s) \end{aligned} \tag{11}$$

$$\begin{aligned} V_{Lqs}(s) &= \left(R_s + sL_q\right)\, I_{qs}(s) \\ &= V_{qs}(s) - P\omega_r(s)\, L_d\, I_{ds}(s) \end{aligned} \tag{12}$$

After computing (8), the interface filter voltage drop V_{Lfd} & V_{Lfq} within the PMa-SynRG emulator in the *dq*-frame also requires to be converted into the V_{od} & V_{oq} modulation voltage in the *dq*-frame for driving the emulated converter. As the interface filter represents an inductor, the V_{od} & V_{oq} can be computed by (13) & (14), respectively:

$$\begin{aligned} V_{od}(s) &= V_{ds}(s) - \left(sL_f + R_f\right)\, I_{ds}(s) + PL_f\omega_r(s)\, I_{qs}(s) \\ &= V_{ds}(s) - V_{Lfd}(s) + PL_f\omega_r(s)\, I_{qs}(s) \end{aligned} \tag{13}$$

$$\begin{aligned} V_{oq}(s) &= V_{qs}(s) - \left(sL_f + R_f\right)\, I_{qs}(s) - PL_f\omega_r(s)\, I_{ds}(s) \\ &= V_{qs}(s) - V_{Lfq}(s) - PL_f\omega_r(s)\, I_{ds}(s) \end{aligned} \tag{14}$$

Via combining (11), (12), (13), and (14), equations (15) & (16) are acquired, demonstrating the computation from the V_{ds} & V_{qs} to the V_{od} & V_{oq}.

$$\begin{aligned} V_{od}(s) = &\left(V_{ds}(s) + PL_f\omega_r(s)I_{qs}(s)\right) \\ &- \left(V_{ds}(s) + PL_q\omega_r(s)I_{qs}(s) - P\omega_r\lambda_{PM}\right) G_{rd}(s) \end{aligned} \tag{15}$$

$$\begin{aligned} V_{oq}(s) = &\left(V_{qs}(s) - PL_f\omega_r(s)\, I_{ds}(s)\right) \\ &- \left(V_{qs}(s) - PL_d\omega_r(s)\, I_{ds}(s)\right) G_{rq}(s) \end{aligned} \tag{16}$$

Fig. 10 depicts the LIR signal flow. As illustrated, this flow is distributed into parts 1, 2, and 3. Part 1represents the computation from the V_s input voltage to the PMa-SynRG

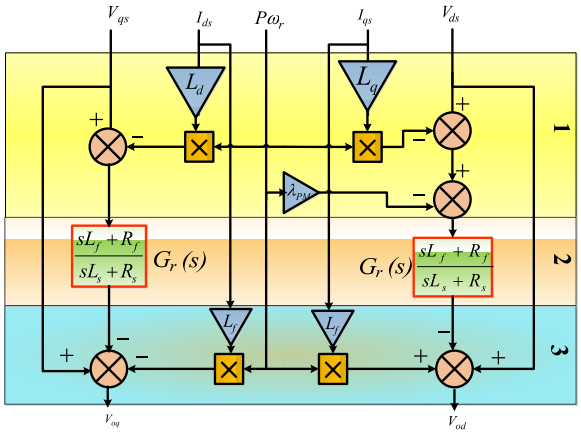

FIGURE 10. The signal flow of the LIR in the *dq*-frame.

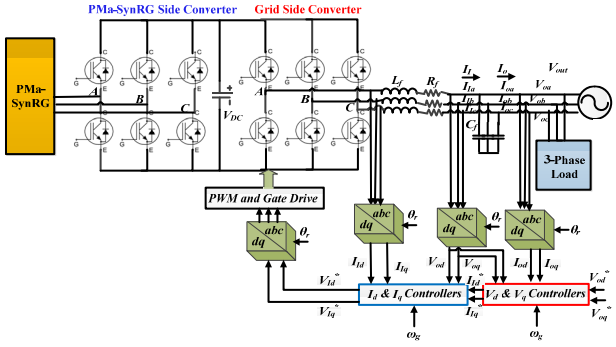

FIGURE 11. Operating the voltage source converter as a voltage amplifier with voltage control approach.

stator voltage drop V_{Ls}, meanwhile part 3 represents the computation from the interface filter voltage drop V_{Lf} to the V_o modulation voltage to drive the emulated converter. The TF $G_r(s)$ through part 2 is discretized via Tustin Method in [29]as well as implemented like a digital filter in the digital processors.

B. VOLTAGE SOURCE CONVERTER CONTROL

The voltage source converter can supply the power to the three-phase load, as a result of flowing the current, a phase shift and a voltage drop are occurred between the system output and the terminals of the inverter voltage. This phase shift and the voltage drop rely on the current of the load which it can be determined via the characteristics of the three-phase load. Modulation command to the three-phase converter can be adapted through the real-time. This can be fulfilled via the usage of vector control approach illustrated in Fig. 11.

Referring to Fig. 11, the control can sustain the output voltage V_{out} at a target value. This value can be defined through the PMa-SynRG model. In addition, the equivalent impedance of the *LC* filter should be less than the PMa-SynRG impedance for guaranteeing that the existence of *LC* filter will not minimize the available bandwidth for emulating the dynamics of the PMa-SynRG.

In addition, the current and the voltage control loops in the *dq*-reference frame are utilized for regulating the frequency

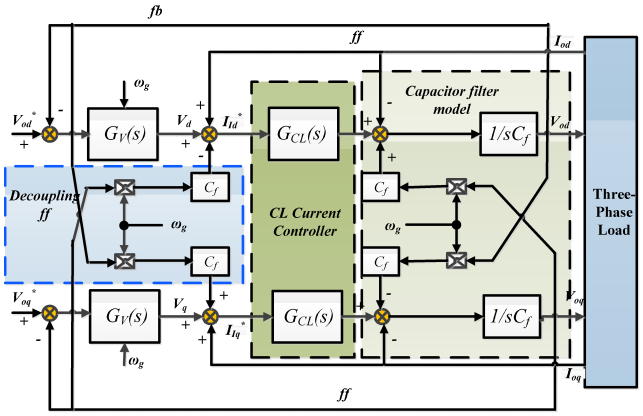

FIGURE 12. Block diagram of voltage source converter with voltage control approach.

and the load voltage to target commanded values. The target frequency ω_g is set consistent with the frequency of the PMa-SynRG. For transforming *abc* to *dq*-reference frames, the angle θ_r is acquired from (4). The target output reference V_{od}^* as well as V_{oq}^* are set consistent with the PMa-SynRG stator voltages V_d and V_q.

The block diagram of the voltage source converter with the voltage control approach in the *dq*-reference frame and the closed-loop (CL) current controllers connected with the capacitor filter model is illustrated in Fig. 12. For designing the voltage and the current controllers, the system was assumed to be balanced. Consequently, the zero and the negative components are disregarded.

In Fig. 12, the terms of the feed-forward (*ff*) components $C_f\,\omega_g V_{oq}$ and $C_f\,\omega_g V_{od}$ are summed for eliminating the cross- coupling between V_{oq} and V_{od}. As depicted, both V_{oq} and V_{od} can be controlled via the signals of I_{Iq}^* and I_{Id}^* which are produced from voltage control approach. Moreover, the *ff* of the load current I_{oq} and I_{od} are summed to the process of the voltage controller for reducing the load current on the capacitor voltage.

Referring to Fig. 7, I_{Iq}^* & I_{Id}^* can be represented in *s*-domain as illustrated in (17):

$$\begin{bmatrix} I_{Iq}^*(s) \\ I_{Id}^*(s) \end{bmatrix} = \begin{bmatrix} V_q(s) \\ V_d(s) \end{bmatrix} + C_f \begin{bmatrix} \omega_g V_{od}(s) \\ -\omega_g V_{oq}(s) \end{bmatrix} + \begin{bmatrix} I_{oq}(s) \\ I_{od}(s) \end{bmatrix} \quad (17)$$

$$\begin{bmatrix} V_q(s) \\ V_d(s) \end{bmatrix} = G_V(s) \begin{bmatrix} V_{oq}^*(s) - V_{oq}(s) \\ V_{od}^*(s) - V_{od}(s) \end{bmatrix} \quad (18)$$

where $G_v(s)$ denotes the voltage controller. Indeed, the load voltage dynamics can be calculated in the state space via employing Kirchhoff's current law on the node of the capacitor and this can be expressed by (19):

$$\frac{dV_{o,abc}}{dt} = \frac{(I_{I,abc} - I_{o,abc})}{C_f} \quad (19)$$

By taking Laplace transformations for (18), yields:

$$s \begin{bmatrix} V_{oq}(s) \\ V_{od}(s) \end{bmatrix} = \begin{bmatrix} -\omega_g V_{od}(s) \\ \omega_g V_{oq}(s) \end{bmatrix} + \frac{1}{C_f} \begin{bmatrix} I_{Iq}(s) - I_{oq}(s) \\ I_{Id}(s) - I_{od}(s) \end{bmatrix} \quad (20)$$

The I_{Iq}, I_{Id} as well as I_{Iq}^*, I_{Id}^* relationship can be expressed by (21):

$$\begin{bmatrix} I_{Iq}(s) \\ I_{Id}(s) \end{bmatrix} = G_{CL}(s) \begin{bmatrix} I_{Iq}^*(s) \\ I_{Id}^*(s) \end{bmatrix} \tag{21}$$

As $G_{CL}(s)$ denotes the TF of the current controller CL and can be expressed by (22):

$$G_{CL}(s) = \frac{G_I(s)G_P(s)}{L_f s + R_f + G_I(s)G_P(s)} \tag{22}$$

where $G_I(s)$ denotes the current controller open-loop TF, whereas, the $G_P(s)$ represents the TF of the pulse width modulation (PWM) block.

For the controlling the I_d and I_q currents, proportional-integral (PI) controllers are employed and can be presented by (23):

$$G_I(s) = K_p + \frac{K_I}{s} \tag{23}$$

where K_p and K_I denote the proportional and the integral gains parameters of the PI controller. The CL current controller is designed for obtaining bandwidth with superior rejection of high-frequency disturbances and a unity DC gain,

According to the voltage controller design, the $I_{Iq}(s)$ and $I_{Id}(s)$ from (21) can be substituted in (20), thus, (24) is obtained:

$$\begin{bmatrix} V_{oq}(s) \\ V_{od}(s) \end{bmatrix} = G_K(s) \begin{bmatrix} V_{oq}^*(s) \\ V_{od}^*(s) \end{bmatrix} + C_f H_K(s) \begin{bmatrix} -\omega_g V_{od}(s) \\ \omega_g V_{oq}(s) \end{bmatrix} - H_K(s) \begin{bmatrix} I_{oq}(s) \\ I_{od}(s) \end{bmatrix} \tag{24}$$

where $G_K(s)$ represents the CL voltage TF and is expressed by (25):

$$G_K(s) = \frac{G_I(s)G_V(s)}{C_f s + G_I(s)G_V(s)} \tag{25}$$

whereas $H_K(s)$ represents the TF of the system output impedance. According to (24), the output voltage is a function of both the load current as well as the reference voltage.

According to the voltage controller, $G_V(s)$ is designed for allowing the load voltages effectively track the reference voltages with rapid transient performance during the nonlinear and linear loading conditions. Consequently, when the voltage source converter is connected to a linear load leading to sinusoidal PMa-SynRG stator voltages and load currents, thus, V_d and V_q will be DC components.

In the voltage control loop, PI controllers are employed. This controller is designed with large gain at the zero frequency for disregarded the steady-state error. Thus, $G_K(s)$ will approach to unity. Though, when the voltage source converter is connected to a nonlinear load, the PMa-SynRG stator voltages will be distorted because of the harmonics of the load current. Moreover, this will produce AC components in V_d and V_q at definite frequencies correlated to the low order and fundamental harmonics in the stationary reference frame. Therefore, the PI controllers are employed for eliminating the steady-state error as it is designed with large gain at 0 Hz.

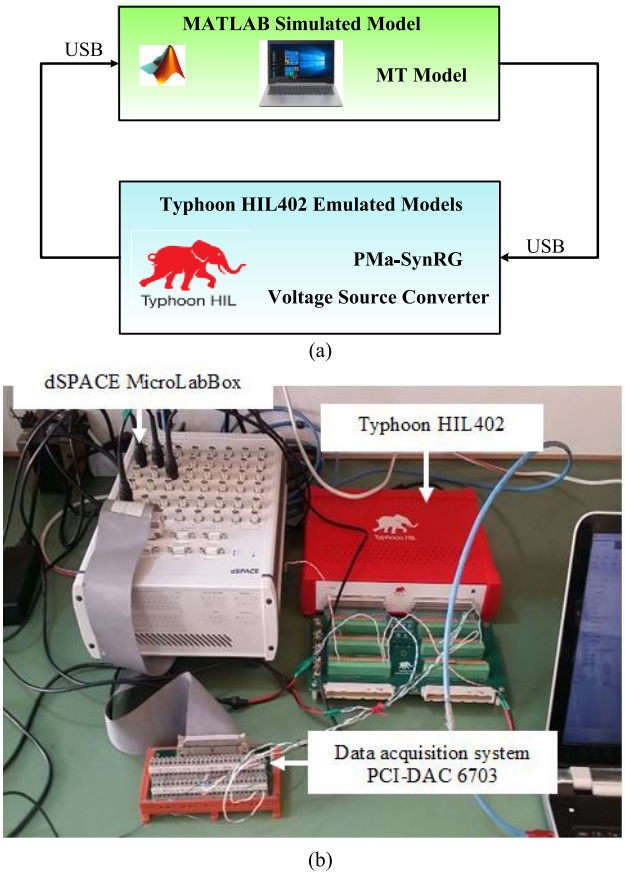

FIGURE 13. PHIL real-time setup for emulating PMa-SynRG and voltage source converter.(a) PHIL architecture. (b) PHIL setup.

In order to attain proper reference voltage tracking performance, the PI controller is equipped with PIR controller and it is used in the voltage control loop. The TF of the PIR controller can be expressed by (26):

$$G_V(s) = K_{PV} + \frac{K_{IV}}{s} + \frac{2K_{mV}\omega_c s}{s^2 + 2\omega_c s + \omega_0^2} \tag{26}$$

where K_{PV}, K_{IV}, and K_{mV} denote the proportional, integral, and the resonant components of the PIR voltage controller, respectively. Meanwhile, ω_0 as well as ω_c represent the resonant and cutoff frequencies, respectively. The voltage controller can introduce large gain at ω_0, thus, the steady-state error will be very small. In addition, ω_0 should be repeatedly tuned as the emulator is designed to operate during variable frequency condition. Indeed, the PIR voltage controller can compensate the double harmonic.

IV. PERFORMANCE EVALUATION

Fig. 13 depicts the experimental setup for the proposed emulated voltage source converter-based PMa-SynRG (Table 1) using the LIR on the PHIL. The proposed system emulates a 3-phase 8 HP PMa-SynRG driven via a 10 HP dynamometer along with the voltage source converter. The MT dynamics has been simulated using MATLAB R2019b according to the mathematical model introduced by Rowen in [28] and

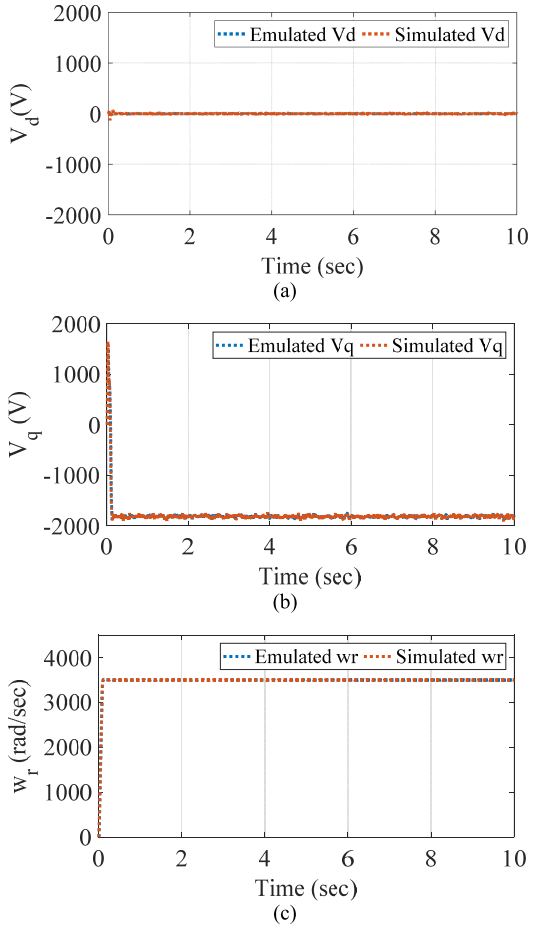

FIGURE 14. Comparison between emulated signals using PHIL and simulated signals using MATLAB during MT starting-up with speed reference of 3500 rad/sec for (a) V_d. (b) V_q. (c) Rotor speed of MT system.

interfaced with the PHIL via the USB. As depicted, the lab setup comprises the emulated model of the PMa-SynRG based on the LIR on PHIL (Typhoon HIL 402) connected to the dSPACE MicroLabBox for processing the control of the voltage source converter which is implemented using MATLAB R2019b environment. The parameters of the voltage amplifier are illustrated in Table 2. Moreover, the *LC* filter network is employed with inductance of 3 mH as well as a capacitance of 4 μF. This network should have adequate bandwidth for replicating the system electrical transients.

The main target of the experimental investigation is to emulate the dynamics of the PMa-SynRG based on the LIR via controlling the output terminal characteristics of voltage source converter, which is connected to the neutral point clamped (NPC) converter for DC rectification. The coupling between NPC and power factor corrected load controls is replaced by a variable resistive load R_L for simplicity.

A. MT STARTING-UP WITH HALF OF REFERENCE SPEED

In order to investigate the performance of the proposed emulated PMa-SynRG, the PMa-SynRG based on the LIR has been simulated via MATLAB R2019b and the emulated

TABLE 2. Parameters of voltage amplifier.

Power switches	IGBT	Filter capacitance	4 µF
DC bus voltage	2000 V	Switching frequency	10 kHz
Filter inductance	3 mH	Filter cut-off frequency	15 kHz

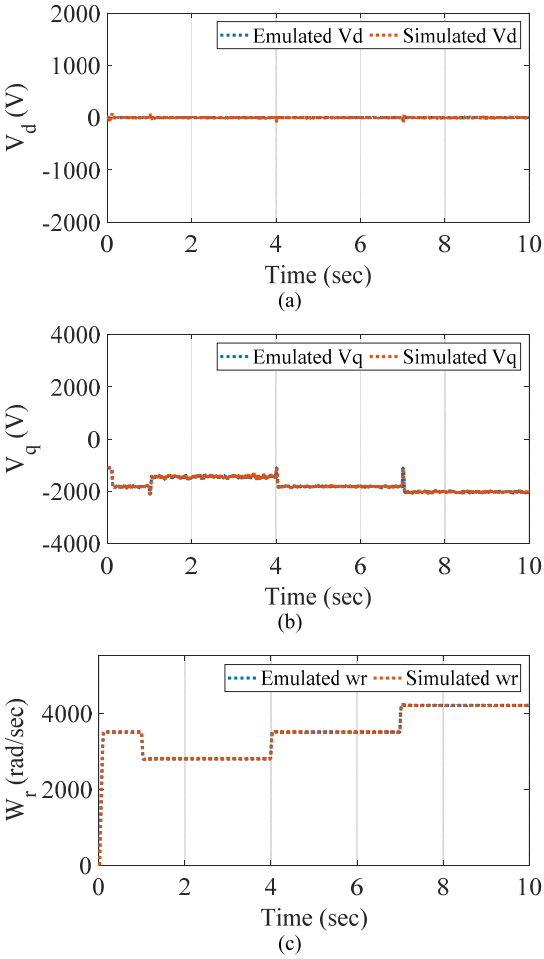

FIGURE 15. Comparison between emulated signals using PHIL and simulated signals using MATLAB during the speed reference change for (a) V_d. (b) V_q. (c) Rotor speed of MT system.

model performance has been compared with the simulated one. This comparison has been performed according to the signals of V_q, V_d, and ω_r with reference speed of 3500 rad/sec. Fig. 14a depicts the variation of V_d which is nearly zero as the rated output voltage is about 1700 V. As shown in Figs. 14a, 14b, and 14c, the emulated signals are the same as the simulated signals effectively, thus, the error between the emulated signals of V_q, V_d, and ω_r and the simulated signals is small.

B. EMULATED PMa-SynRG BASED ON THE LIR WITH PIR CONTROLLER PERFORMANCE DURING REFERENCE SPEED CHANG

In this test, the rotor reference speed is changed to85% of rated speed at t = 0-1 sec, then at t = 1-4 sec the reference speed reaches 70% of rated speed. Afterwards, at t = 4-7 sec, the speed reaches 85% of rated speed, then at t = 7-10 sec,

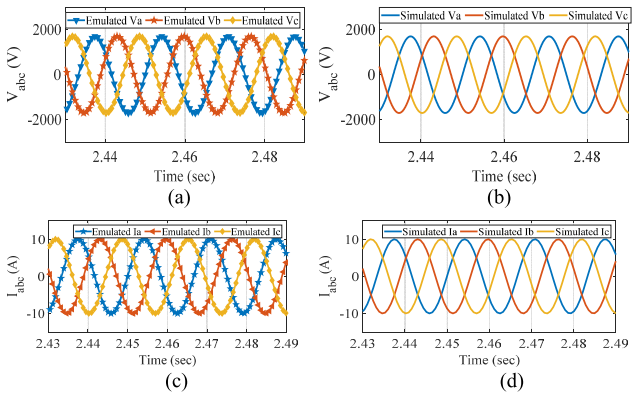

FIGURE 16. PMa-SynRG three-phase stator voltages and current using PHIL and MATLAB Simulink at reference speed of 3500 rad/sec under linear load condition. (a) Emulated V_{abc}. (b) Simulated V_{abc}. (c) Emulated I_{abc}. (d) Simulated I_{abc}.

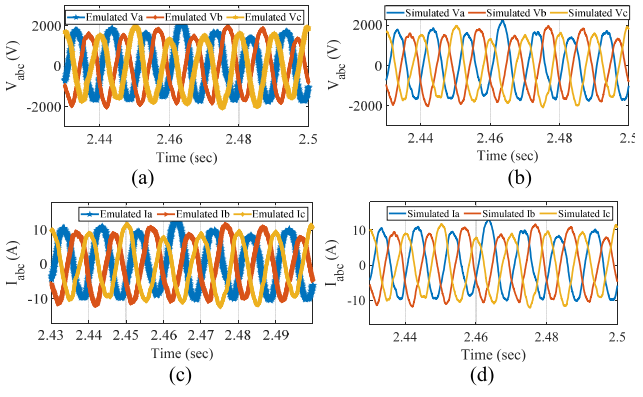

FIGURE 17. PMa-SynRG three-phase stator voltages and current using PHIL and MATLAB Simulink at reference speed of 3500 rad/sec under nonlinear load condition. (a) Emulated V_{abc}. (b) Simulated V_{abc}. (c) Emulated I_{abc}. (d) Simulated I_{abc}.

it reaches to its rated value. Fig. 15 depicts the comparison between emulated and simulated signals of V_q, V_d, and ω_r. It is noted that the emulated signals are the same as the simulated signals, consequently, the error between the emulated signals of V_q, V_d, and ω_r and the simulated signals is minimal.

C. EMULATED PMa-SynRG BASED ON THE LIR WITH PIR CONTROLLER PERFORMANCE UNDER NONLINEAR AND LINEAR LOADS

In order to investigate the effectiveness of the proposed emulated PMa-SynRG based on the LIR, linear/nonlinear loads have been connected to the PMa-SynRG emulator. Fig.16 depicts the three-phase stator voltages and currents in the steady-state for the emulated and simulated PMa-SynRG V_{abc} and I_{abc} signals when a linear load is used in this test with reference speed of 3500 rad/sec.

The emulated signals are obtained using the PHIL SCADA. As depicted, when a linear load is employed, the PMa-SynRG stator voltages and currents are sinusoidal waveforms. However, when the load is nonlinear, the PMa-SynRG three-phase voltage and currents are not pure sinusoidal as illustrated in Fig. 17. Also, it is noted that the emulated PMa-SynRG three-phase stator voltages and currents are identical with the simulated PMa-SynRG stator voltages and currents which can prove the effectiveness of PHIL to emulate PMa-SynRG successfully. Moreover, the emulated V_{abc} and I_{abc} waveforms with the proposed PIR controller approach properly track the simulated PMa-SynRG model.

D. EMULATED PMa-SynRG BASED ON THE LIR WITH PIR CONTROLLER PERFORMANCE UNDER VIRTUAL IMPEDANC

In order to investigate the effectiveness of the proposed emulated PMa-SynRG based on the LIR, virtual impedance consists of a series resistive capacitive (RC) filter is employed to investigate its effect on the PMa-SynRG's performance. This test is performed also to confirm the influence on the PMa-SynRG emulator precision in case the load current has

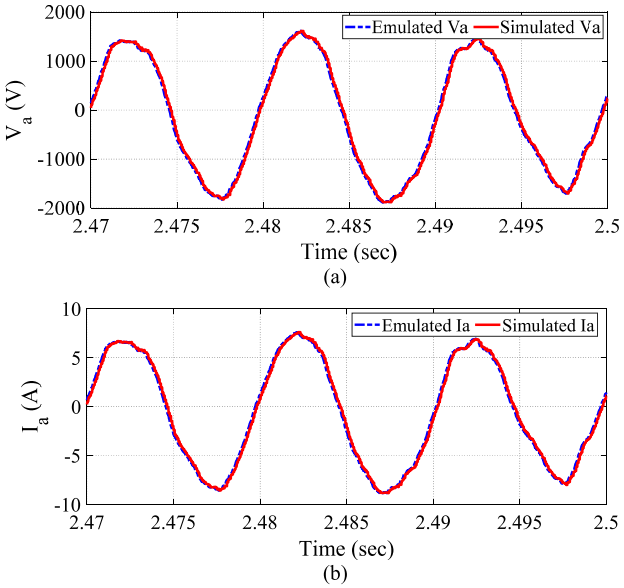

FIGURE 18. PMa-SynRG three-phase stator voltages and current using PHIL and MATLAB Simulink at reference speed of 3500 rad/sec and using virtual impedance. (a) Emulated and Simulated V_a. (b)Emulated and Simulated I_a.

low-order harmonic components. The values of the virtual impedance are 5Ω and 5mF.

Fig. 18 depicts the performances of the phase voltage and phase current of the PMa-SynRG emulator based on the LIR with the virtual impedance (RC filter). As depicted, the PMa-SynRG model current *is* does not match the emulator load current *io*. The maximum absolute error is 0.08 p.u. for the voltage and 0.42 p.u. for the current waveforms. Therefore, the *RC* filter introduces a large error when the load waveform presents fast varying components.

V. CONCLUSION

This paper presented the emulation of a high-speed MT PMa-SynRG based on the linear impedance regulator using the PHIL platform for renewable energy experiments. The main

contribution is in designing an emulated model for PMa-SynRG which can replicate the real hardware PMa-SynRG on the PHIL. The LIR has been employed for replacing the current control loop in the emulator system. The LIR reshaped the *s*-domain performances of the emulated converter with the interface filter. The PMa-SynRG emulator based on the LIR can act more properly in emulation, as well as is expected to afford more precise along with flexible solutions to the emulation and investigations for highly complex applications of power electronics systems. This paper also presented the interfacing between the three-phase voltage source converter with three-phase LC network for filtering the voltages of the PWM which are switched to the filtered terminal voltages with actual hardware of power factor corrected load for emulating the dynamics of the MT output using the mathematical model of the MT. Moreover, the vector control approach using the PIR controller design steps were also introduced in this paper. The PMa-SynRG emulator performance using the PIR controller has been compared with the simulated PMa-SynRG model using MATLAB environment and it was experimentally investigated. The experimental validation results have been presented under reference speed change and under nonlinear/linear loads conditions. These results endorsed that the proposed PMa-SynRG emulator can perform well with high precision for both nonlinear/linear loading conditions. Consequently, the proposed PMa-SynRG emulator can be used as an efficient test bed for investigating and emerging hydrokinetic/WECSs.

REFERENCES

[1] Y. Shi, J. Wang, and B. Wang, "Electromagnetic-thermal coupled simulation under various fault conditions of a triple redundant 9-phase PMASynRM," *IEEE Trans. Ind. Appl.*, vol. 56, no. 1, pp. 128–137, Jan. 2020.

[2] A. Tap, L. Xheladini, M. Yilmaz, M. Imeryuz, T. Asan, and L. T. Ergene, "Comprehensive design and analysis of a PMaSynRM for washing machine applications," *IET Electr. Power Appl.*, vol. 12, no. 9, pp. 1311–1319, Nov. 2018.

[3] B. Wang, J. Wang, A. Griffo, and B. Sen, "Experimental assessments of a triple redundant nine-phase fault-tolerant PMA SynRM drive," *IEEE Trans. Ind. Electron.*, vol. 66, no. 1, pp. 772–783, Jan. 2019.

[4] J. Baek, M. M. Rahimian, and H. A. Toliyat, "Optimal design and comparison of stator winding configurations in permanent magnet assisted synchronous reluctance generator," in *Proc. IEEE Int. Electr. Mach. Drives Conf.*, Miami, FL, USA, May 2009, pp. 732–737.

[5] I. Boldea, L. Tutelea, and C. I. Pitic, "PM-assisted reluctance synchronous Motor/Generator (PM-RSM) for mild hybrid vehicles: Electromagnetic design," *IEEE Trans. Ind. Appl.*, vol. 40, no. 2, pp. 492–498, Mar. 2004.

[6] M. D. Nardo, G. L. Calzo, M. Galea, and C. Gerada, "Design optimization of a high-speed synchronous reluctance machine," *IEEE Trans. Ind. Appl.*, vol. 54, no. 1, pp. 233–243, Jan. 2018.

[7] F. Gao, X. Zheng, S. Bozhko, C. I. Hill, and G. Asher, "Modal analysis of a PMSG-based DC electrical power system in the more electric aircraft using eigenvalues sensitivity," *IEEE Trans. Transp. Electrific.*, vol. 1, no. 1, pp. 65–76, Jun. 2015.

[8] J. Pippola, I. Vaalasranta, T. Marttila, J. Kiilunen, and L. Frisk, "Product level accelerated reliability testing of motor drives with input power interruptions," *IEEE Trans. Power Electron.*, vol. 30, no. 5, pp. 2614–2622, May 2015.

[9] B. Ji, V. Pickert, W. Cao, and B. Zahawi, "*In situ* diagnostics and prognostics of wire bonding faults in IGBT modules for electric vehicle drives," *IEEE Trans. Power Electron.*, vol. 28, no. 12, pp. 5568–5577, Dec. 2013.

[10] W. Liu, X. Xie, X. Zhang, and X. Li, "Frequency-coupling admittance modeling of converter-based wind turbine generators and the Control-Hardware-in-the-Loop validation," *IEEE Trans. Energy Convers.*, vol. 35, no. 1, pp. 425–433, Mar. 2020.

[11] T. Liang, Q. Liu, and V. R. Dinavahi, "Real-time Hardware-in-the-Loop emulation of high-speed rail power system with SiC-based energy conversion," *IEEE Access*, vol. 8, pp. 122348–122359, 2020.

[12] S. Chakraborty, M. Mazuela, D.-D. Tran, J. A. Corea-Araujo, Y. Lan, A. A. Loiti, P. Garmier, I. Aizpuru, and O. Hegazy, "Scalable modeling approach and robust Hardware-in-the-Loop testing of an optimized interleaved bidirectional HV DC/DC converter for electric vehicle drivetrains," *IEEE Access*, vol. 8, pp. 115515–115536, 2020.

[13] A. Javadi, M. Abarzadeh, L.-A. Gregoire, and K. Al-Haddad, "Real-time HIL implementation of a single-phase distribution level THSeAF based on D-NPC converter using proportional-resonant controller for power quality platform," *IEEE Access*, vol. 7, pp. 110372–110386, 2019.

[14] K. S. Amitkumar, R. Thike, and P. Pillay, "Linear amplifier-based Power-Hardware-in-the-Loop emulation of a variable flux machine," *IEEE Trans. Ind. Appl.*, vol. 55, no. 5, pp. 4624–4632, Sep. 2019.

[15] M. Fischer, R. Malić, N. Tröster, J. Ruthardt, and J. Roth-Stielow, "Design of a three-phase 100 a linear amplifier for power-hardware-in-the-loop machine emulation," *J. Eng.*, vol. 2019, no. 17, pp. 4041–4044, Jun. 2019.

[16] R. S. Kaarthik, J. Maisonneuve, and P. Pillay, "Real-time emulation of a pressure-retarded osmotic power generation system," *IEEE Trans. Ind. Appl.*, vol. 53, no. 6, pp. 5768–5776, Nov. 2017.

[17] W. Guo, W. Ge, X. Lu, and H. Li, "Short-term load forecasting of virtual machines based on improved neural network," *IEEE Access*, vol. 7, pp. 121037–121045, 2019.

[18] A. A. Al-Aghbari and M. E. S. Elrabaa, "Cloud-based FPGA custom computing machines for streaming applications," *IEEE Access*, vol. 7, pp. 38009–38019, 2019.

[19] R. Nair and G. Narayanan, "Emulation of wind turbine system using vector controlled induction motor drive," *IEEE Trans. Ind. Appl.*, vol. 56, no. 4, pp. 4124–4133, Aug. 2020.

[20] O. Vodyakho, M. Steurer, C. S. Edrington, and F. Fleming, "An induction machine emulator for high-power applications utilizing advanced simulation tools with graphical user interfaces," *IEEE Trans. Energy Convers.*, vol. 27, no. 1, pp. 160–172, Mar. 2012.

[21] F. Alvarez-Gonzalez, A. Griffo, B. Sen, and J. Wang, "Real-time Hardware-in-the-Loop simulation of permanent-magnet synchronous motor drives under stator faults," *IEEE Trans. Ind. Electron.*, vol. 64, no. 9, pp. 6960–6969, Sep. 2017.

[22] G. Zhao and S. Zhang, "Development of permanent magnet synchronous motor RCP based on Hardware-in-the-Loop simulation," in *Proc. IEEE Int. Conf. Mechatronics Autom. (ICMA)*, Changchun, China, Aug. 2018, pp. 264–269.

[23] L. Zhang and H. Guo, "Power Hardware-in-the-loop emulation system for permanent magnet synchronous machines," in *Proc. 22nd Int. Conf. Electr. Mach. Syst. (ICEMS)*, Harbin, China, Aug. 2019, pp. 1–6.

[24] A. Hasanzadeh, C. S. Edrington, N. Stroupe, and T. Bevis, "Real-time emulation of a high-speed microturbine permanent-magnet synchronous generator using multiplatform Hardware-in-the-Loop realization," *IEEE Trans. Ind. Electron.*, vol. 61, no. 6, pp. 3109–3118, Jun. 2014.

[25] M. Ashourianjozdani, L. A. C. Lopes, and P. Pillay, "Power electronic converter based PMSG emulator: A testbed for renewable energy experiments," *IEEE Trans. Ind. Appl.*, vol. 54, no. 4, pp. 3626–3636, Jul. 2018.

[26] R. S. Kaarthik, K. S. Amitkumar, and P. Pillay, "Emulation of a permanent-magnet synchronous generator in real-time using power Hardware-in-the-Loop," *IEEE Trans. Transp. Electrific.*, vol. 4, no. 2, pp. 474–482, Jun. 2018.

[27] T.-F. Chan, W. Wang, and L.-L. Lai, "Permanent-magnet synchronous generator supplying an isolated load," *IEEE Trans. Magn.*, vol. 46, no. 8, pp. 3353–3356, Aug. 2010.

[28] W. I. Rowen, "Simplified mathematical representations of heavy-duty gas turbines," *J. Eng. Power, Trans. ASME*, vol. 105, no. 4, pp. 865–869, Oct. 1983.

[29] D. Yang and X. Wang, "Unified modular state-space modeling of grid-connected voltage-source converters," *IEEE Trans. Power Electron.*, vol. 35, no. 9, pp. 9700–9715, Sep. 2020.

FAYEZ F. M. EL-SOUSY (Member, IEEE) received the B.Sc. degree in electrical engineering from Menoufia University, Al Minufya, Egypt, in 1988, and the M.Sc. and Ph.D. degrees in electrical engineering from Cairo University, Giza, Egypt, in 1994 and 2000, respectively. Since 1990, he has been with the Department of Power Electronics and Energy Conversion, Electronics Research Institute, Giza, where he is currently a Full Professor. From August 1995 to June 2003, he was with the Department of Electrical Engineering, October Six University, Giza. From April 2004 to February 2007, he was a Postdoctoral Visiting Researcher with the Graduate School of Information Science and Electrical Engineering, Kyushu University, Fukuoka, Japan. From 2007 to 2010, he was with the Department of Electrical Engineering, College of Engineering, King Saud University, Riyadh, Saudi Arabia. From 2010 to 2014, he was with the Department of Electrical Engineering, College of Engineering, Salman bin Abdulaziz University, Al-Kharj, Saudi Arabia. Since 2014, he has been with the Department of Electrical Engineering, College of Engineering, Prince Sattam bin Abdulaziz University, Saudi Arabia. His research interests are in the areas of modeling and control of motor drives, motion-control systems, wind energy systems, digital signal processing-based computer control systems, computational intelligent of power electronics and electric drives, intelligent control theories, including fuzzy logic, neural networks, and wavelets, nonlinear control and optimal control, and robust control. He is currently interested in the intelligent control of the Maglev vehicle transportation system.

GHADA A. ABDEL AZIZ (Member, IEEE) received the B.Sc. and M.Sc. degrees in electrical engineering from Minofiya University, Egypt, in 2006 and 2009, respectively, and the Ph.D. degree in electrical engineering from Cairo University, Egypt, in 2015. From 2006 to 2008, she was a TA with several academic institutions in Egypt. Since 2009, she joined the Electronics Research Institute (ERI), Egypt, as a Research Assistant, where she has been a Researcher since 2015. She was awarded as the best researcher at ERI due to her published papers at the IEEE, in 2018 and 2019, respectively. Her current research interests include control of electrical machines, electrical machines drives, fault-tolerant control, fault-tolerant design of the electric machine, and power electronics in renewable energy systems. She is a Reviewer at IEEE Access, IEEE Transaction on Energy Conversion, and IEEE Transaction on Industrial Electronics.

MAHMOUD AMIN (Senior Member, IEEE) received the Ph.D. degree in electrical engineering from Florida International University, Miami, FL, USA, in 2012. He is currently an Associate Professor with the ECE Department, Manhattan College, New York, NY, USA; a Courtesy Research Associate Professor at Florida International University; and a Researcher with the Electronic Research Institute. His research interests include applications of power electronics in renewable energy systems, microgrids, adjustable speed drives, and smart grid. He has one edited book, one book chapter, and over 60 articles in professional journals and refereed international conference proceedings. He is the Director of the Sustainable Energy Systems Laboratory, Manhattan College. He is a recipient of the IEEE PES GM 2010 Paper Contest Award, the Main Award in Typhoon HIL's 10 for 10 Program, the 7×24 University Challenge Award, the Intel FPGA University Program Grant Award, and the Grand Challenge $2M Grant. He is an Editor for the *Machines MDPI*, and a Guest Editor for the IEEE Transactions on Energy Conversion and IEEE Transactions on Magnetics.

KHALED GABER received the B.Sc. and M.Sc. degrees in electronics and communications engineering from the Arab Academy for Science, Technology and Maritime Transport (AASTMT), Egypt, in 2005 and 2011, respectively, and the Ph.D. degree in electronics and communications engineering from Al-Azhar University, Cairo, Egypt, in 2020. He is participating in several academic research activities at the National Research Center (NRC) and Electronics Research Institute (ERI) Cairo, Egypt. Since 2005, he started his career in different sectors of telecom industries. He is holding many certificates in the project and program management, including PRINCE2 Agile®Foundation & Practitioner, Synergy®V.6 Foundation & Practitioner, ITIL V4®, and Certified Scrum Master®. He is currently the Project Director and International B2GaaS Program Manager in one of the leading multinational telecom firms. His current research interests include MEMS sensors, attitude determination in small satellites, cybersecurity, as well as control of electronic and communication systems.

OSAMA A. MOHAMMED (Life Fellow, IEEE) is currently a Distinguished Professor of Electrical Engineering and the Associate Dean of Research at the College of Engineering and Computing, Florida International University, Miami, FL, USA, where he is also the Director of the Energy Systems Research Laboratory. His research interests include computational electromagnetics, design optimization of EM devices, as well as physics-based modeling in electric drives and power electronic systems. His research also involves diagnostics through EM signatures, EMI, energy cyber-physical systems, and smart grid communications. He is recently involved in utilizing wideband gap devices and packaging designs for improved power densities and thermal management for transportation electrification and renewable energy and storage applications. He has more than 15 patents awarded or filed and has published more than 700 articles in refereed journals and other IEEE refereed international conference records. He is an elected fellow of the Applied Computational Electromagnetic Society. He received the IEEE PES Cyril Veinott Electromechanical Energy Conversion Award and the 2012 Outstanding Research Award from Florida International University, and the 2017 Outstanding Doctoral Mentor. He was named the Distinguished Professor at FIU in 2018. He has served or currently serving as the International Steering Committee Chair for the IEEE IEMDC, the IEEE CEFC, ACES, and COMPUMAG. He has also served as the general chair for more than ten major international conferences and was the President of the Applied Computational Electromagnetic Society (ACES).